

## APPENDIX A: FINITE DIFFERENCES DISCRETIZATION OF THE HESSIAN TERM

Equation 8 includes the following term involving the Hessian matrix:

$$\begin{aligned} \mathcal{K} : \nabla \nabla \Phi = & \mathcal{K}_{11} \frac{\partial^2 \Phi}{\partial x^2} + \mathcal{K}_{22} \frac{\partial^2 \Phi}{\partial y^2} + \mathcal{K}_{33} \frac{\partial^2 \Phi}{\partial z^2} + \\ & (\mathcal{K}_{12} + \mathcal{K}_{21}) \frac{\partial^2 \Phi}{\partial x \partial y} + (\mathcal{K}_{13} + \mathcal{K}_{31}) \frac{\partial^2 \Phi}{\partial x \partial z} + (\mathcal{K}_{23} + \mathcal{K}_{32}) \frac{\partial^2 \Phi}{\partial y \partial z}, \end{aligned} \tag{19}$$

where we have taken advantage of the symmetry of the Hessian tensor (the normalized conductivity tensor, on the other hand, is asymmetric). Let us take, for example, the term  $\frac{\partial^2 \Phi}{\partial x \partial y}$ : applying the chain rule with the intermediate computational coordinates  $(\xi, \eta, \zeta)$  yields

$$\begin{aligned} \frac{\partial^2 \Phi}{\partial x \partial y} = & \frac{\partial^2 \xi}{\partial x \partial y} \frac{\partial \Phi}{\partial \xi} + \frac{\partial^2 \eta}{\partial x \partial y} \frac{\partial \Phi}{\partial \eta} + \frac{\partial^2 \zeta}{\partial x \partial y} \frac{\partial \Phi}{\partial \zeta} + \\ & + \left( \frac{\partial \xi}{\partial x} \frac{\partial \xi}{\partial y} \right) \frac{\partial^2 \Phi}{\partial \xi^2} + \left( \frac{\partial \eta}{\partial x} \frac{\partial \eta}{\partial y} \right) \frac{\partial^2 \Phi}{\partial \eta^2} + \left( \frac{\partial \zeta}{\partial x} \frac{\partial \zeta}{\partial y} \right) \frac{\partial^2 \Phi}{\partial \zeta^2} + \\ & + \left( \frac{\partial \xi}{\partial x} \frac{\partial \eta}{\partial y} + \frac{\partial \eta}{\partial x} \frac{\partial \xi}{\partial y} \right) \frac{\partial^2 \Phi}{\partial \xi \partial \eta} + \left( \frac{\partial \xi}{\partial x} \frac{\partial \zeta}{\partial y} + \frac{\partial \zeta}{\partial x} \frac{\partial \xi}{\partial y} \right) \frac{\partial^2 \Phi}{\partial \xi \partial \zeta} + \left( \frac{\partial \eta}{\partial x} \frac{\partial \zeta}{\partial y} + \frac{\partial \zeta}{\partial x} \frac{\partial \eta}{\partial y} \right) \frac{\partial^2 \Phi}{\partial \eta \partial \zeta}. \end{aligned} \tag{20}$$

Here, the derivatives of the computational coordinates  $(\xi, \eta, \zeta)$  correspond to Jacobian matrix elements and derivatives of them; they depend only on the employed mesh, are constant throughout the simulation, and are computed with FD schemes. All second derivative terms are zero in uniform meshes, while crossed first-derivative terms (like  $\partial \xi / \partial y$ ) are zero in rectangular meshes. The node coefficients for the derivatives of  $\Phi$  appearing in Eq. 20 and involving  $\eta$  and  $\xi$  and are shown in Fig. 9; analogous coefficients apply to derivatives involving  $\zeta$ . The proposed FD schemes are 2<sup>nd</sup> order in accuracy.

Similar expansions apply to the other 5 derivatives of Eq. 19, by simply substituting  $\partial x \partial y$  with the corresponding physical coordinates. Finally, the normalized conductivity tensor  $\mathcal{K}$  in Eq. 19 is evaluated at the central node where the operator is being discretized (i.e. at the center node of the schemes shown in Fig. 9).

## APPENDIX B: GLOBAL CONTINUITY ERROR IN THE FD SCHEME

In the FD formulation, the discretized equation is elliptic and requires a different way of computing the right hand side term and imposing the boundary conditions, which can ultimately result in an artificial current continuity error, appearing at the Dirichlet node as a current sink/source. First, for what concerns the RHS, contrary to the FV formulation, the FD approach computes it by taking the divergence of a known vector of PIC magnitudes,  $\nabla \cdot (\mathbf{j}_i - \mathcal{K} \cdot \mathbf{j}_c) / \sigma_e$  (see Eq. 8). This operation is, of course, subject to a truncation error (being the known PIC vector a non trivial and noisy function in general), which can yield an overall unbalance of the electric current generated inside the simulation domain volume (compared to the one entering through the boundaries).

Second, while in the FV method, the BCs on the electric current are imposed explicitly (i.e. setting the values of the unknown currents with Eq. 16), in the FD approach, the directional derivative of  $\Phi$  along the

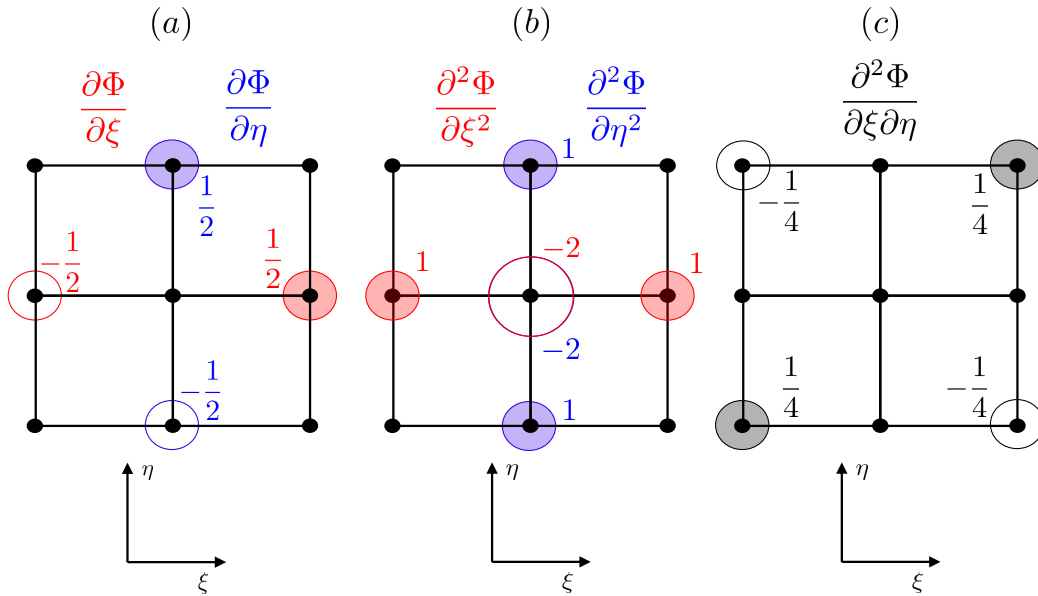


**Figure 9.** Centered finite differences schemes for different computational derivatives of the thermalized potential: (a) simple derivatives, (b) second derivatives and (c) mixed derivatives. Nodes are shown by black dots. The node coefficient is shown by a filled/empty circle depending on whether it is positive/negative, with its exact value indicated and proportional to the circle area.

direction  $\mathcal{K}^T \cdot \mathbf{1}_n$  is actually imposed (see Eq. 11). In magnetized scenarios, as  $\chi$  grows, this direction can become parallel to certain domain boundaries resulting in an ill-conditioned linear system.

The truncation error effects on the RHS have been assessed with a set of 5 simplified test cases, whose simulation geometry is depicted in Fig. 10, being the physical domain a cube of side 1m. Local ambipolar current conditions have been considered at the domain boundaries, with different functional dependencies of  $\mathbf{j}_i = \mathbf{j}_c$  on  $z$  alone (uniform properties along  $x, y$ ).

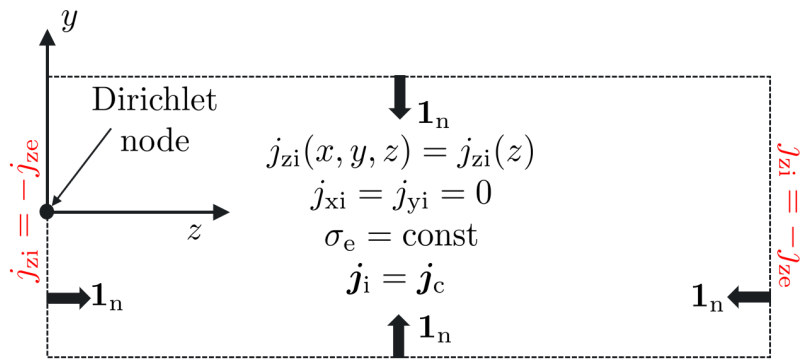


**Figure 10.** Simulation domain considered for the RHS discretization error cases. A zero magnetic induction field is assumed.

The electron conductivity  $\sigma_e$  is uniform, and the 5 different analytical profiles for  $j_{zi}, j_{zc}$  are shown in Fig. 11. Tab. 4 summarizes, for 2 different mesh resolutions (20x20x20 nodes, and 40x40x40 nodes), the main results in terms of the relative continuity error, defined as  $\varepsilon_{I,FD} = |I_{z,Dir}| / I_{inj,i}$ , and representing the ratio between the total electric current in through the Dirichlet node (absolute error), and the total electron/ion current crossing  $z_0$ .

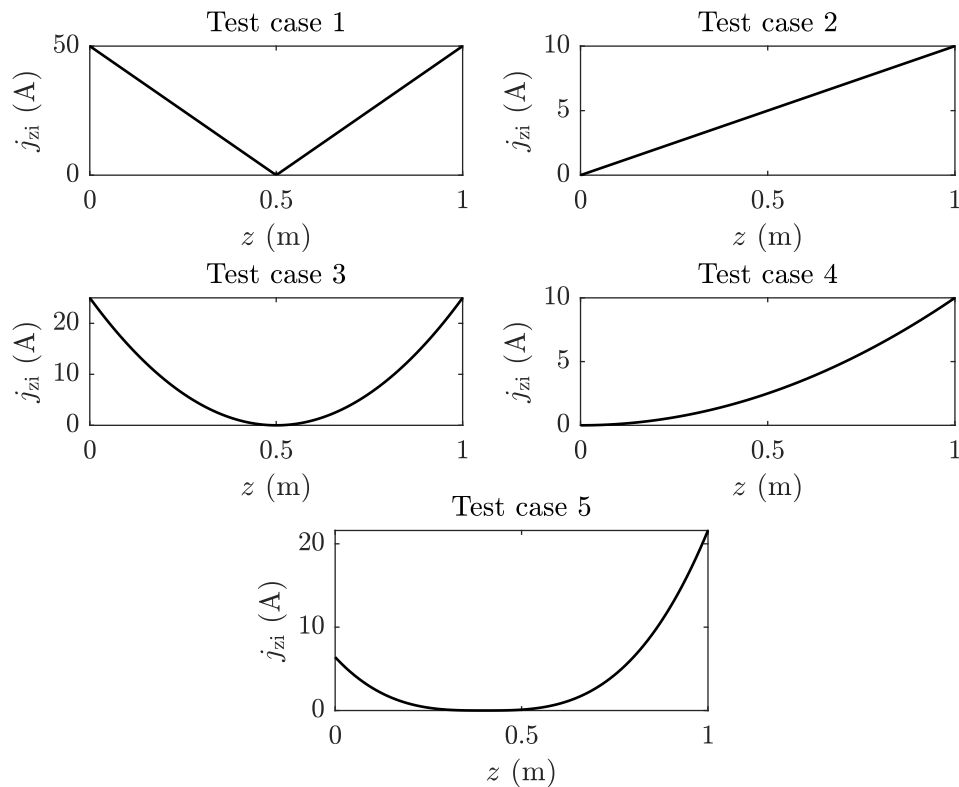


**Figure 11.** Visual representation of the functions used to define  $j_{zi}$  in each test case.

The considered simplifications imply that the only LHS contribution is due to the Hessian term. From the performed tests, it is evident that, since a 2<sup>nd</sup> order accuracy FD scheme is adopted for the computation of the RHS divergence term, any function of order greater than 2 inside the divergence operator of the RHS is affected by a truncation error. This results in an artificial electric current at the only node where the continuity equation is not imposed, thus at the Dirichlet reference node. Moreover, results show that, this artificial current scales exactly with the square of the mesh size (see Tab. 4, test case 5). As expected, the same behavior is observed when the function is exponential (derivable) or with discontinuities (non derivable). However, if the function is symmetric (i.e. in test case 1), the discretization errors compensate each other and cancel out integrally (the derivative error has opposite signs at symmetric locations), so that no continuity error is observed either.

Clearly, in hybrid PIC-fluid simulations, the noise and non trivial current density profiles from the PIC always feature truncation error effects, so that a current continuity error always arises, as shown in Tab. 2.

**Table 4.** Relative percentage of global continuity errors  $\varepsilon_{I,FD} = |I_{Dir}|/I_{inj,i}$ , obtained by imposing analytical profiles of  $j_{zi}$  to the FD fluid solver in unmagnetized case. Mesh 2 features double the number of nodes per direction, compared to mesh 1.

Test case	$j_{zi}$ profile	$\varepsilon_{I,FD}$ mesh 1	$\varepsilon_{I,FD}$ mesh 2
1	Linear symmetric along $z$ (triangular)	0.0	0.0
2	Linear monotonic (asymmetric along $z$ )	0.0	0.0
3	Quadratic (symmetric along $z$ )	0.0	0.0
4	Quadratic (asymmetric along $z$ , shifted)	0.0	0.0
5	Polynomial of order $\geq 3$ and asymmetric ( $j_{zi}(z) = 100 \cdot  z - \bar{z} ^3$ )	0.6%	0.15%